Nano-X-ray Absorption Spectroscopy of Single Co-Implanted ZnO Nanowires

ARTICLE *in* NANO LETTERS · DECEMBER 2011

Impact Factor: 13.59 · DOI: 10.1021/nl202799e · Source: PubMed

5 AUTHORS, INCLUDING:

Gema Martinez-Criado
European Synchrotron Radiation Facility
113 PUBLICATIONS **983** CITATIONS
SEE PROFILE

Carsten Ronning
Friedrich Schiller University Jena
275 PUBLICATIONS **4,535** CITATIONS
SEE PROFILE

NANO LETTERS

LETTER

pubs.acs.org/NanoLett

Nano-X-ray Absorption Spectroscopy of Single Co-Implanted ZnO Nanowires

J. Segura-Ruiz,*[,†] G. Martínez-Criado,[†] M. H. Chu,[†] S. Geburt,[‡] and C. Ronning[‡]

[†]European Synchrotron Radiation Facility, Experiments Division, 38043 Grenoble, France

[‡]Institute of Solid State Physics, University of Jena, D-07743 Jena, Germany

Supporting Information

ABSTRACT: We report on the local structure of single Co-implanted ZnO nanowires studied using a hard X-ray nanoprobe. X-ray fluorescence maps show uniform Zn and Co distributions along the wire within the length scale of the beam size. The X-ray fluorescence data allow the estimation of the Co content within the nanowire. Polarization dependent X-ray absorption near edge structure shows no structural disorder induced neither in the radial nor axial directions of the implanted nanowires after subsequent annealing. Co^{2+} ions occupy Zn sites into the wurtzite ZnO lattice. Extended X-ray absorption fine structure data reveal high structural order in the host lattice without distortion in their interatomic distances, confirming the recovery of the radiation damaged ZnO structure through thermal annealing.

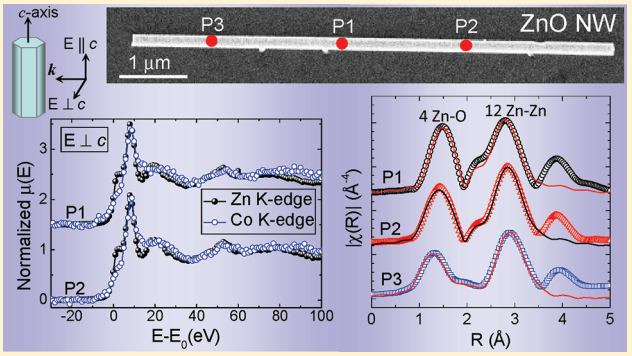

KEYWORDS: EXAFS, XANES, nanowires, ZnO, dilute magnetic semiconductors

Determining the local order of individual nanostructures is crucial to understand their behavior in the spintronics nanodevices.[1−3] In particular, Co-doped ZnO nanowires (NWs) offer unique advantages owing to their large geometrical aspect ratio and predicted room-temperature ferromagnetism.[4,5] In addition to spintronic applications, transitions involving degenerated Co 3d-shell states within the ZnO could be used in optoelectronic devices.[6] However, controlled doping of semiconductor NWs with transition metals (TM) during growth remains a challenge. For instance, the doping of NWs by metal−organic chemical vapor deposition,[7] molecular beam epitaxy,[8] or hot-walled pulsed laser deposition,[9] gives origin to a high density of structural defects (e.g., edge dislocations and stacking faults), inhomogeneous dopant distribution and secondary phases. Ion implantation is an alternative that allows a better control of both concentration and distribution of TM ions.[10] Determining the doping homogeneity and local order of individual implanted nanostructures is crucial to understand their behavior in spintronics nanodevices. Although there are many reports about ensembles of NWs, it remains controversial whether the incorporation of Co in individual NWs is substitutional as in bulk crystals or thin films, without the formation of metallic clusters or precipitates.[11,12] The average local atomic structure and secondary phases in ensembles of NWs have already been studied by X-ray absorption near edge structure (XANES) and extended X-ray absorption fine structure (EXAFS).[13,14] However, the examination of single NWs remains an experimental challenge. Alternatively, the long-range order in single nanostructures has been analyzed by X-ray nanodiffraction,[15] three-dimensional strain images of single NWs have been obtained by coherent X-ray diffraction imaging,[16] and the 3D structure of nanoscale crystals by X-ray Fourier transform holography.[17] Moreover, we have recently reported the application of synchrotron fluorescence nanoimaging to single NWs,[18,19] but the X-ray absorption acquisitions have been mostly limited by the beam instability during the energy scan and chromaticity of the nanofocusing lens. In this work, a Kirkpatrick−Baez mirror based nanoprobe with scanning X-ray fluorescence (XRF) capability was used to explore phase separation effects and short-range order in single Co implanted ZnO NWs. In addition, the linear polarization of the synchrotron nanobeam made our study not only element specific but also capable of detecting preferentially oriented defects induced by the ion implantation process.[20]

In this Letter, we describe the investigation of ZnO NWs grown on p-Si (100) substrates using vapor−liquid−solid process. The main NW axis is parallel to the *c*-axis of the wurtzite structure. The Co ions were implanted using a dose of 1.57×10^{16} cm^{-2} with ion energies ranging from 60 to 300 keV to obtain a homogeneous concentration profile. After the Co implantation, the NWs were annealed at 750 °C in air during four hours to recover from the radiation induced lattice damage. More details about growth and implantation processes can be found elsewhere.[6,21] For the X-ray based analysis, the

Received: August 12, 2011
Revised: October 2, 2011
Published: October 18, 2011

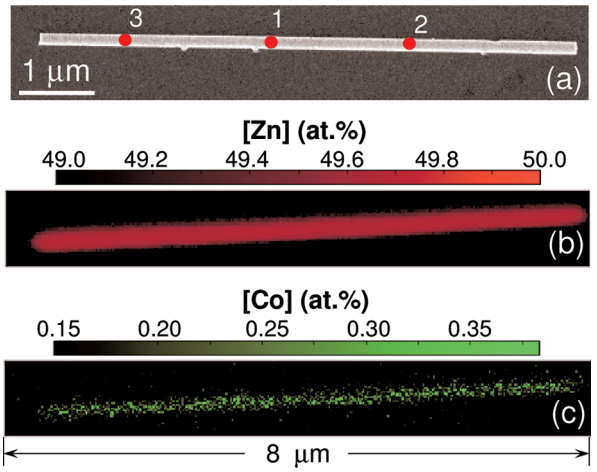

Figure 1. (a) SEM image of the single Co implanted NW. Elemental maps collected at 12 keV for Zn (b) and Co (c) with the respective atomic fraction estimated from the XRF quantification.

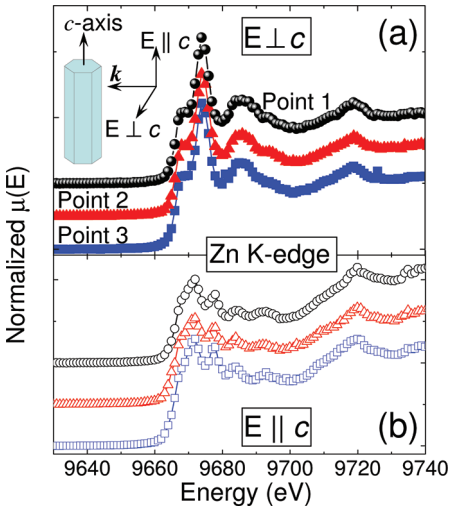

Figure 2. Zn K edge XANES spectra recorded along the NW with the *c*-axis oriented perpendicular (a), and parallel (b) to the electric field vector of the X-ray nanobeam. For clarity, the spectra were shifted vertically.

NWs were transferred to a clean p-Si (100) substrate via imprint. The X-ray absorption measurements were carried out at the hard X-ray nanoprobe beamline ID22 of the European Synchrotron Radiation Facility.[22] The monochromatic X-ray beam was focused to 100 × 100 nm^2 spot size with ~10^{11} ph/s using a pair of Kirkpatrick−Baez Si mirrors. The intensity of the incident beam was monitored with a gas filled ionization chamber. The XRF signal was collected at 15° with respect to the substrate surface with a Si drift detector. The XRF maps were taken at 12 keV with a pixel size of 25 × 25 nm^2 and an accumulation time of 500 ms per pixel. The information depths of Co and Zn fluorescence photons were about 8.0 and 4.3 μm at 12 keV, respectively.[23] Using the PyMca program,[24] the XRF spectra were fitted to quantify the elemental composition. XANES and EXAFS data were recorded in XRF mode with a step size of 1 eV and integration times determined by the counting statistics. The data analysis was performed using the IFEFFIT package.[25]

Figure 1a shows the scanning electron microscopy (SEM) image of a single NW with diameter and length of 180 nm and 7 μm, respectively. The positions indicated by 1, 2, and 3 correspond to the areas where XANES and EXAFS spectra were recorded. Figure 1b,c shows the elemental maps of Zn and Co with the respective concentrations estimated from the XRF quantification.[26] The average concentrations of Co and Zn are (0.3 ± 0.1) and (49.7 ± 0.1) atom %, respectively. These values are in good agreement with those obtained from simulations using the IRADINA Monte Carlo code,[27] which takes the nanowire geometry fully into account. Within our detection limits, the observed content variations are due to signal-to-noise statistics rather than changes in the Co and Zn fractions. The maps indicate homogeneous distributions of Co and Zn along the NW without any signature of clusters or nanoaggregates.

Taking advantage of the high spatial resolution and the linear polarization of the X-ray beam, Zn K edge XANES spectra recorded along the NW are shown in Figure 2a. The *c*-axis of the NW is oriented perpendicular to the electric field vector of the synchrotron radiation. Due to the scalar product between the photon polarization vector ($\mathbf{e}$) and the position vector of the electron ($\mathbf{r}$) in the matrix element of the absorption cross section: $\mathbb{M} = \langle \phi_{1s} | \mathbf{e} \cdot \mathbf{r} | \phi_f \rangle$, XANES spectra in wurtzite ZnO depend on the crystallographic orientation.[28] Thus, if the electric field of the absorbed photons is perpendicular to the *c*-axis ($\mathbf{E} \perp c$), transitions from 1s to p_{xy} states are allowed. Therefore, under our experimental configuration, the XANES data probe the symmetry of the *ab*-plane, namely p_{xy} conduction band states. The spectral features in Figure 2a reflect the typical wurtzite structure of the ZnO lattice.[29] No signatures of Zn metallic precipitates after the ion implantation process are observed in the spectra. According to the line shapes and peaks energies, there is no structural disorder in the radial direction along the implanted NW. For the axial direction, Figure 2b displays the XANES data from the NW with its *c*-axis oriented parallel to the electric field vector of the X-ray beam. Thus, the XANES data probe the symmetry of the *c*-plane, namely p_z conduction band states. Again, the spectra exhibit the peaks associated to the hexagonal structure, without any evidence of lattice damage along the NW. Our findings reveal the high structural order of the host lattice along both radial and axial directions.

Figure 3a shows the XANES spectra around the Zn K edge (solid circles) and Co K edge (open circles) at points 1 and 2. To enable the comparison between Zn and Co XANES spectra, the energy has been rescaled to the respective absorption K edges calculated from the first derivative of the XANES signal. Despite the low Co content, the quality of the XANES data around the Co K edge reproduces well the oscillations of the Zn K edge spectra at both points, with minor differences above 70 eV. Co ions seem to be incorporated into the wurtzite host lattice on the Zn sites. To gain further insight into the Co chemical configuration, Figure 3b shows the average XANES spectrum of the NW around the Co K edge (solid circles). For comparison, we have included the Co K edge XANES of a high quality wurtzite $Zn_{0.9}Co_{0.1}O$ epitaxial film taken from ref 29 (open circles), a mixed valence Co_3O_4 sample (open triangles), and a metallic Co foil (open squares). The good match between the NW and ZnCoO data suggests oxidation state 2+ for Co ions. Metallic Co and/or mixed valence Co_3O_4 contributions are not clearly visible. The weak pre-edge peak around 7710 eV arises from the hybridization of the Co 3d and 4p orbitals states induced by the tetrahedral crystal field within the

dx.doi.org/10.1021/nl202799e |*Nano Lett.* 2011, 11, 5322–5326

noncentrosymmetric ZnO structure.[14,30] While a strong pre-edge peak is associated with the existence of pure CoO particles as a secondary phase,[14] our result supports that Co has been substitutionally incorporated into the wurtzite ZnO lattice.

In order to confirm the local structure, EXAFS data around the Zn K edge were acquired at different positions along the NW. Figure 4a plots the k^3-weight EXAFS oscillations accompanied by their best fits in the interval [0−8.1 Å^{-1}] using a Hanning window. The data analysis was carried out by ab initio modeling of the absorption cross section using the FEFF code.[31] Theoretical backscattering amplitudes and phase shifts for all single and multiple scattering paths were calculated using hexagonal ZnO model clusters (a = 3.289 Å and c = 5.315 Å).[32] The ARTEMIS routine[25] was exploited to fit the data in R space within the window [1.0−3.7 Å], which included the first and second coordination shells. On the basis of previous X-ray diffraction data,[33] a fixed coordination of 4 O nearest neighbor atoms and 12 Zn second-nearest-neighbor atoms was applied. We have fitted the interatomic distances (R_i) and Debye−Waller (DW) factors (σ_i^2) of the various atomic shells, fixing the amplitude s_0^2 = 0.7307 as determined from the metallic Zn foil. The values of the structural parameters extracted from the curve fits are reported in Table 1.

Figure 4b shows the corresponding magnitude of the Fourier transforms (FTs) of the EXAFS functions. The spectra show two dominant peaks related to the first O- and second Zn-shells, which are expected in the wurtzite model. All points show the same contributions with a slight decrease in the first shell amplitude as a function of the position. In general, within the experimental accuracy, there is no change in the first and second neighbor distances along the NW. Note that the Zn−O and Zn−Zn spacings are equal to those of pure ZnO (1.98 and 3.25 Å[34]), without any evidence of amorphization. The undistorted cation−anion first neighbor distance also reflects the low Co content estimated by XRF in the implanted ZnO NW (Figure 1). For points 2 and 3, the apparent reduced amplitude of the nearest O-neighbor peak is accounted for by the higher static disorder; namely, increase of their corresponding DW factors. The data analysis suggests that there is no local atomic distortion around the Zn sites, although there is an increase in the width of the interatomic distance distribution, as measured by the EXAFS DW factor. The overall EXAFS results do not indicate any significant contribution from common defects generated by the implantation process, e.g., secondary phases, vacancy accumulations and interstitials. This confirms

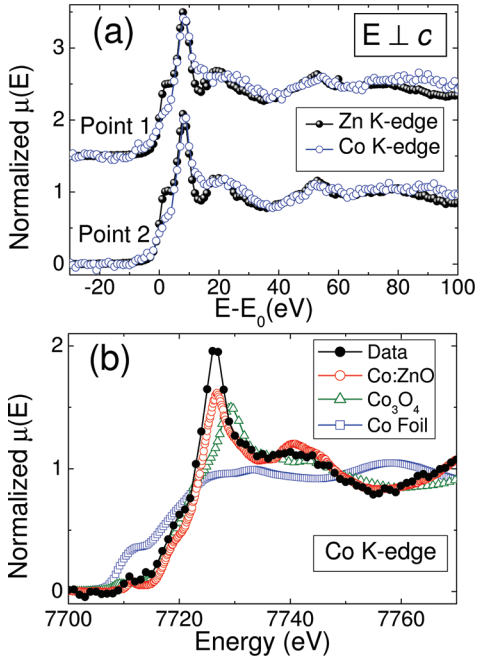

Figure 3. (a) XANES spectra around the Zn K edge (solid circles) and Co K edge (open circles) taken at points 1 and 2. The energy has been rescaled to the respective absorption K edges. (b) Average XANES spectrum of the NW around the Co K edge (solid circles), a high quality wurtzite $Zn_{0.9}Co_{0.1}O$ epitaxial film taken from ref 29 (open circles), a mixed valence Co_3O_4 sample (open triangles), and a metallic Co foil (open squares).

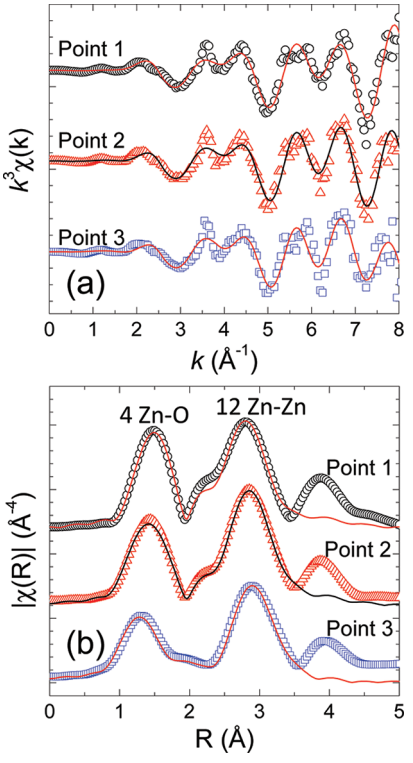

Figure 4. (a) k^3-weight EXAFS oscillations (open symbols) accompanied by their best fits (solid lines) in the interval k = 0−8.1 Å^{-1}. (b) Magnitude of the FTs of the EXAFS functions (open symbols) and their best fits (solid lines). For clarity, the spectra were shifted vertically.

Table 1. Summary of the Interatomic Distances (R_i), Debye−Waller (DW) Factors (σ_i^2) of the Various Atomic Shells, and the R-Factors Obtained from the Fittings of the FT EXAFS Fixing s_0^2 = 0.7307 As Determined from the Metallic Zn Foil

point	R_{Zn-O} (Å)	$\sigma^2_{Zn-O} \times 10^{-3}$ (Å^2)	R_{Zn-Zn} (Å)	$\sigma^2_{Zn-Zn} \times 10^{-3}$(Å^2)	R
1	1.97 ± 0.02	2.3 ± 1.6	3.25 ± 0.02	5.0 ± 1.4	0.016
2	1.98 ± 0.02	3.7 ± 1.6	3.25 ± 0.01	4.5 ± 1.3	0.011
3	1.98 ± 0.02	9.3 ± 2.0	3.25 ± 0.01	7.4 ± 1.5	0.011

dx.doi.org/10.1021/nl202799e |Nano Lett. 2011, 11, 5322–5326

the good recovery of the radiation damaged ZnO lattice through the thermal annealing.

The overall EXAFS results obtained in these NWs are in agreement with what we have observed in 4 atom % Co implanted ZnO NW by transmission electron microscope (TEM).[6] There, secondary phases in the NWs after annealing were not observed, although the structural damage created by the ion implantation process was not completely removed by annealing. However, to further corroborate our findings, new TEM images were acquired in several 1 atom % Co implanted NWs. In Supplementary Figures S1 and S2 in Supporting Information we show midmagnification and high-resolution TEM images of single NWs, along with their electron diffraction patterns and the fast Fourier transform (FFT) of selected areas. The high-resolution TEM images show a perfect recovered ZnO lattice without any evidence of extended defects or secondary phases. Furthermore, the FFT images exhibit sharp spots, which are signatures of a nearly perfect wurtzite single crystal after the annealing. The spacing between the (0002)-planes determined from the TEM images is around 0.52 nm, which is in good agreement with the values obtained from the fittings of our EXAFS results. In some NWs, a very low density of stacking faults and dislocations remaining after the annealing were observed. This fact could explain the higher static disorder observed by EXAFS in some points of the NW. Therefore, the overall TEM results fully support the recovery of the radiation damaged ZnO lattice through the thermal annealing evidenced in our EXAFS results.

In summary, we have studied the local structure of single Co implanted ZnO NWs using a hard X-ray nanoprobe. Elemental maps showed Zn and Co ions homogeneously distributed along the NW. From the XRF spectra an estimation of the Co content in the wire was reported, with an average [Co] = (0.3 ± 0.1) atom %. Polarization dependent XANES showed that there was no structural disorder induced neither in the radial nor axial directions of the implanted NWs. XANES around the Co K edge displayed the substitutional incorporation of Co^{2+} ions into the Zn sites of the wurtzite host lattice. EXAFS data analysis supported the tetrahedral configuration of Zn in the hexagonal host lattice without pronounced distortion in the interatomic distances of the two nearest neighbor shells. Our EXAFS results gave no evidence of large structural defects induced in the ZnO host lattice by the Co incorporation and confirm the annealing mediated recovery of the ZnO structure. Although the presence of defects cannot be completely ruled out, within the sensitivity of our experimental techniques neither secondary phases or oxygen vacancies were observed. Our findings are fully supported by the TEM analysis of implanted single NWs.

■ ASSOCIATED CONTENT

Supporting Information. Figures showing midmagnification and high-resolution TEM images of Co implanted ZnO NWs, along with their electron diffraction pattern and the fast Fourier transform (FFT) of selected areas. This material is available free of charge via the Internet at http://pubs.acs.org.

■ AUTHOR INFORMATION

Corresponding Author
*E-mail: seguraru@esrf.fr.

■ ACKNOWLEDGMENT

The authors thank Steffen Milz and Irina Snigireva for their help with the TEM and SEM measurements, respectively. We thank Remi Tocoulou and Peter Cloetens for their help and the ESRF for the beam time allocated. We also thank Claudia Schnohr for the valuable discussions and Gary Admans for the critical reading of the manuscript. This work has been partially supported by the NANOWIRING Marie Curie ITN (EU project no. PITN-GA-2010-265073).

■ REFERENCES

(1) Tulapurkar, A. A.; Suzuki, Y.; Fukushima, A.; Kubota, H.; Maehara, H.; Tsunekawa, K.; Djayaprawira, D. D.; Watanabe, N.; Yuasa, S. *Nature* **2005**, *438*, 339–342.
(2) Sankey, J. C.; Braganca, P. M.; Garcia, A. G. F.; Krivorotov, I. N.; Buhrman, R. A.; Ralph, D. C. *Phys. Rev. Lett.* **2006**, *96*, 227601.
(3) Mourachkine, A.; Yazyev, O. V.; Ducati, C.; Ansermet, J.-P. *Nano Lett.* **2008**, *8*, 3683–3687.
(4) Heo, Y. W.; Norton, D.; Tien, L.; Kwon, Y.; Kang, B.; Ren, F.; Pearton, S.; LaRoche, J. *Mater. Sci. Eng., R* **2004**, *47*, 1–47.
(5) Cui, J. B.; Gibson, U. J. *Appl. Phys. Lett.* **2005**, *87*, 133108.
(6) Müller, S.; Zhou, M.; Li, Q.; Ronning, C. *Nanotechnology* **2009**, *20*, 135704.
(7) Chen, C.-H.; Chang, S.-J.; Chang, S.-P.; Li, M.-J.; Chen, I.-C.; Hsueh, T.-J.; Hsu, A.-D.; Hsu, C.-L. *J. Phys. Chem. C* **2010**, *114*, 12422–12426.
(8) Urban, A.; Malindretos, J.; Seibt, M.; Rizzi, A. *Nano Lett.* **2011**, *11*, 398–401.
(9) Song, Y.-W.; Kim, K.; Ahn, J. P.; Jang, G.-E.; Lee, S. Y. *Nanotechnology* **2009**, *20*, 275606.
(10) Chen, I.-J.; Ou, Y.-C.; Wu, Z.-Y.; Chen, F.-R.; Kai, J.-J.; Lin, J.-J.; Jian, W.-B. *J. Phys. Chem. C* **2008**, *112*, 9168–9171.
(11) Cui, J.; Gibson, U. *Phys. Rev. B* **2006**, *74*, 045416.
(12) Liao, L.; Li, J. C.; Wang, D. F.; Liu, C.; Peng, M. Z.; Zhou, J. M. *Nanotechnology* **2006**, *17*, 830.
(13) Yuhas, B. D.; Fakra, S.; Marcus, M. A.; Yang, P. *Nano Lett.* **2007**, *7*, 905–909.
(14) Busgen, T.; Hilgendorff, M.; Irsen, S.; Wilhelm, F.; Rogalev, A.; Goll, D.; Giersig, M. *J. Phys. Chem. C* **2008**, *112*, 2412–2417.
(15) Hrauda, N.; Zhang, J.; Wintersberger, E.; Etzelstorfer, T.; Mandl, B.; Stangl, J.; Carbone, D.; Holý, V.; Jovanović, V.; Biasotto, C.; Nanver, L. K.; Moers, J.; Grützmacher, D.; Bauer, G. *Nano Lett.* **2011**, *11*, 2875–2880.
(16) Xiong, G.; Huang, X.; Leake, S.; Newton, M. C.; Harder, R.; Robinson, I. *New J. Phys.* **2011**, *13*, 033006.
(17) Chamard, V.; Stangl, J.; Carbone, G.; Diaz, A.; Chen, G.; Alfonso, C.; Mocuta, C.; Metzger, T. H. *Phys. Rev. Lett.* **2010**, *104*, 165501.
(18) Segura-Ruiz, J.; Martínez-Criado, G.; Sans, J. A.; Tucoulou, R.; Cloetens, P.; Snigireva, I.; Denker, C.; Malindretos, J.; Rizzi, A.; Gomez-Gomez, M.; Garro, N.; Cantarero, A. *Phys. Status Solidi RRL* **2011**, *5*, 95–97.
(19) Chu, M. H.; Segura-Ruiz, J.; Martínez-Criado, G.; Cloetens, P.; Snigireva, I.; Geburt, S.; Ronning, C. *Phys. Status Solidi RRL* **2011**, 283–285.
(20) Jian, W. B.; Wu, Z. Y.; Huang, R. T.; Chen, F. R.; Kai, J. J.; Wu, C. Y.; Chiang, S. J.; Lan, M. D.; Lin, J. J. *Phys. Rev. B* **2006**, *73*, 233308.
(21) Ronning, C.; Borschel, C.; Geburt, S.; Niepelt, R. *Mater. Sci. Eng., R* **2010**, *70*, 30–43 (3rd IEEE International NanoElectronics Conference (INEC)).
(22) Tucoulou, R.; Martínez-Criado, G.; Bleuet, P.; Kieffer, I.; Cloetens, P.; Labouré, S.; Martin, T.; Guilloud, C.; Susini, J. *J. Synchrotron Radiat.* **2008**, *15*, 392–398.
(23) Tröger, L.; Arvanitis, D.; Baberschke, K.; Michaelis, H.; Grimm, U.; Zschech, E. *Phys. Rev. B* **1992**, *46*, 3283–3289.

(24) Solé, V.; Papillon, E.; Cotte, M.; Walter, P.; Susini, J. *Spectrochim. Acta, Part B* **2007**, *62*, 63–68.
(25) Newville, M. *J. Synchrotron Radiat.* **2001**, *8*, 322–324.
(26) Somogyi, A.; Martínez-Criado, G.; Homs, A.; Hernandez-Fenollosa, M. A.; Vantelon, D.; Ambacher, O. *Appl. Phys. Lett.* **2007**, *90*, 181129.
(27) Borschel, C.; Ronning, C. *Nucl. Instrum. Methods Phys. Res., Sect. B* **2011**, *269*, 2133–2138.
(28) Stöhr, J. *NEXAFS Spectroscopy*; Springer: Berlin, 1992.
(29) Ney, A.; Ollefs, K.; Ye, S.; Kammermeier, T.; Ney, V.; Kaspar, T. C.; Chambers, S. A.; Wilhelm, F.; Rogalev, A. *Phys. Rev. Lett.* **2008**, *100*, 157201.
(30) Martínez-Criado, G.; Segura, A.; Sans, J. A.; Homs, A.; Pellicer-Porres, J.; Susini, J. *Appl. Phys. Lett.* **2006**, *89*, 061906.
(31) Ankudinov, A. L.; Ravel, B.; Rehr, J. J.; Conradson, S. D. *Phys. Rev. B* **1998**, *58*, 7565–7576.
(32) Cicero, G.; Ferretti, A.; Catellani, A. *Phys. Rev. B* **2009**, *80*, 201304.
(33) Geurts, J.; Schumm, M.; Koerdel, M.; Ziereis, C.; Müller, S.; Ronning, C.; Dynowska, E.; Gołacki, Z.; Szuszkiewicz, W. *Phys. Status Solidi B* **2010**, *247*, 1469–1471.
(34) Decremps, F.; Datchi, F.; Saitta, A. M.; Polian, A.; Pascarelli, S.; Di Cicco, A.; Itié, J. P.; Baudelet, F. *Phys. Rev. B* **2003**, *68*, 10410.

NOTE ADDED AFTER ASAP PUBLICATION

This paper was published on the Web on October 26, 2011. The word "irradiation" has been changed to "radiation" in four places. The correct version was published on November 7, 2011.